

Spheres and Prolate and Oblate Ellipsoids from an Analytical Solution of Spontaneous Curvature Fluid Membrane Model

Quan-Hui Liu^{1,2**}, Zhou Haijun¹, Ji-Xing Liu¹, Ou-Yang Zhong-Can¹

¹*Institute of Theoretical Physics, Academia Sinica, P.O. Box 2735, Beijing, 100080, China*

²*Department of Physics, Hunan University, Changsha, 410082, China*

(February 1, 2008)

An analytic solution for Helfrich spontaneous curvature membrane model (H. Naito, M.Okuda and Ou-Yang Zhong-Can, Phys. Rev. E **48**, 2304 (1993); **54**, 2816 (1996)), which has a conspicuous feature of representing the circular biconcave shape, is studied. Results show that the solution in fact describes a family of shapes, which can be classified as: i) the flat plane (trivial case), ii) the sphere, iii) the prolate ellipsoid, iv) the capped cylinder, v) the oblate ellipsoid, vi) the circular biconcave shape, vii) the self-intersecting inverted circular biconcave shape, and viii) the self-intersecting nodoidlike cylinder. Among the closed shapes (ii)-(vii), a circular biconcave shape is the one with the minimum of local curvature energy.

87.16.Dg, 47.10.Hg, 68.15.+e, 02.40.Hw

I. INTRODUCTION

Why red blood cells under normal physiological conditions take the circular biconcave shape (CBS) but not the spherical shape aroused the long standing curiosity of human being since its first discovery in the seventieth century. Today, physicists ascribe it to the minimization of bending energy of flexible lipid bilayer membrane consisting of amphiphilic molecules. The first successful model revealing the morphology was due to Canham [1] in 1970. However, his theory suffered from the shortcoming that the membrane was assumed to consist of two identical labile surfaces, and both chemical and physical environments between two sides of the membrane were assumed to be identical too. To overcome the shortcoming, Helfrich in 1973 introduced a phenomenological parameter, namely the spontaneous curvature, in describing the more realistic situations: the asymmetry of the two leaflets of the membrane and the chemical or/and physical differences between the interior and exterior membrane [2]. As expected, this model gave more abundant shapes than that of Canham. Based on the numerical integration technique [3], Helfrich spontaneous curvature model yielded a catalog of axisymmetric vesicle shapes: the CBS, the prolate and oblate ellipsoid, etc. More than ten years later, the general equilibrium equation was derived by performing the variation of the Helfrich energy functional [4]. The first triumph of the equation was the prediction of the existence of Clifford torus shape membrane [5] and its subsequent experimental verification [6]. In 1993, the general equation in axisymmetric case was obtained, and it is a complicated third order nonlinear differential equation [7]. An analytic solution capable of representing the CBS [8] was immediately obtained. In the same year, the first integral of the third order nonlinear differential equation was found; then the equation reduced to be a second order one involving a constant of integration C [9]. An interesting fact is that the analytical solution requires a nonvanishing value of C [8,9], whereas only the special case of the second order differential equation with $C = 0$ has been well studied by numerical methods [10]. In 1996, the solution was used to explain the experimentally observed polygonal shape transformation of the CBS [11]. Studies in this paper will show that this solution actually represents a family of shapes in this solution, but in the family, the CBSs have the lower energies and a CBS has the lowest. For convenience, we will call this solution the CBS solution hereafter.

The existence of the analytical CBS solution in Helfrich model proves to be remarkable, because the analytical solutions to a nonlinear theory are rare and precious [12]. In very special cases of $c_0 = \delta p = \lambda = 0$ (cf. following Eq.(1)), the Helfrich energy functional reduces to that for constant curvature surfaces and Willmore surfaces [13], and all known analytical solutions having physical applications in membrane shapes are Delaunay surfaces, sphere, torus [13], and no more [14]. Therefore a systematic study of the CBS solution is necessary. We will find that there are eight types of shapes involved in the solution and the enclosed shapes can be grouped into the prolate or oblate ellipsoid branches. These two branches are bifurcated from a sphere.

The article is organized as follows. In section II, how to obtain the CBS solution from the Helfrich model is outlined. In section III, all typical shapes contained in the CBS solution are plotted and their parameterizations are presented. In section IV, a systematically analysis of the CBS solution is given. In the shape family, there is an shape with minimum energy and in section V this shape is found from the the scale invariance of the local curvature energy. In

section VI, a comparison of our results with the previous experimental and theoretical results is given. In the final section VII, a brief conclusion is given.

II. HELFRICH SPONTANEOUS CURVATURE MODEL AND ITS CBS SOLUTION

Equilibrium shapes of phospholipid vesicles are assumed to correspond to the minimum of the elastic energy of the closed bilayer membrane. The energy functional of Helfrich spontaneous curvature model reads as [2]

$$F = \frac{1}{2}k \int (c_1 + c_2 - c_0)^2 dA + \delta p \int dV + \lambda \int dA, \quad (1)$$

where dA and dV are the surface area and the volume element for the vesicle, respectively, k is an elastic modulus, c_1 and c_2 are the two principal curvatures of the surface, and c_0 is the spontaneous curvature to describe the possible asymmetry of the bilayer membrane. When c_0 is zero Helfrich model reduces to Canham model [1]. The Lagrange multipliers δp and λ take account of the constraints of constant volume and area, which can be physically understood as the osmotic pressure between the ambient and the internal environments, and the surface tension, respectively. The general equilibrium shape equation is [4]

$$\delta p - 2\lambda H + k(2H + c_0)(2H^2 - 2K - c_0H) + 2k\nabla^2 H = 0, \quad (2)$$

where $\nabla^2 = \frac{1}{\sqrt{g}}\partial_i(g^{ij}\sqrt{g}\partial_j)$ is the Laplace-Beltrami operator, g is the determinant of the metric g_{ij} and $g^{ij} = (g_{ij})^{-1}$, $K = c_1 c_2$ is the Gaussian curvature and $H = -(1/2)(c_1 + c_2)$ is the mean curvature. Assuming that the shape has axisymmetry, the general shape equation Eq.(2) becomes a third order nonlinear differential equation [7]

$$\begin{aligned} \cos^3 \psi \left(\frac{d^3 \psi}{dr^3} \right) &= 4 \sin \psi \cos^2 \psi \left(\frac{d^2 \psi}{dr^2} \right) \left(\frac{d\psi}{dr} \right) - \cos \psi \left(\sin^2 \psi - \frac{1}{2} \cos^2 \psi \right) \left(\frac{d\psi}{dr} \right)^3 \\ &+ \frac{7 \sin \psi \cos^2 \psi}{2r} \left(\frac{d\psi}{dr} \right)^2 - \frac{2 \cos^3 \psi}{r} \left(\frac{d^2 \psi}{dr^2} \right) \\ &+ \left[\frac{c_o^2}{2} - \frac{2c_o \sin \psi}{r} + \frac{\lambda}{k} - \frac{\sin^2 \psi - 2 \cos^2 \psi}{2r^2} \right] \cos \psi \left(\frac{d\psi}{dr} \right) \\ &+ \left[\frac{\delta p}{k} + \frac{\lambda \sin \psi}{kr} + \frac{c_o^2 \sin \psi}{2r} - \frac{\sin^3 \psi + 2 \sin \psi \cos^2 \psi}{2r^3} \right], \end{aligned} \quad (3)$$

where r is the distance from the symmetric z axis of rotation, $\psi(r)$ is the angle made by the surface tangent and the r axis as shown in FIG.1. The positive direction of the angle is that the angle measured clockwise from r axis. It is contrary to the usual mathematical convention; therefore, the mean curvature H is $-1/2(\sin \psi/r + d \sin \psi/dr)$, in which $c_1 = \sin \psi/r$ denotes the principal curvature along the parallels of latitude, and $c_2 = d \sin \psi/dr$ denotes that along those of meridian. It is worthy to mention that the spontaneous curvature c_0 carries a sign. When the normal of a surface change its direction, c_1, c_2 and c_0 must change their signs simultaneously. Keeping the directions of r and z as the usual, we have consequently

$$\begin{cases} dz/dr = -\tan \psi(r) \\ z(r) - z(0) = -\int_0^r \tan \psi(r) dr \\ \mathbf{n} = (\sin \psi \cos \phi, \sin \psi \sin \phi, \cos \psi), \end{cases} \quad (4)$$

where \mathbf{n} denotes the normal of the surface and ϕ the azimuthal angle.

For self-consistence, the positive direction of arclength s along the contour in $r - z$ plane is necessary to start from the north pole of the shape. If so, we see that the parameterization for sphere is $\sin \psi(r) = r/R_0$ where $R_0 > 0$ is the radius of the sphere, and our sign convention used in this paper is then compatible with that used in most previous works [3,7,10]. The third order nonlinear differential equation (3) can be simplified to be a second order one [9]

$$\begin{aligned} \cos^2 \psi \frac{d^2 \psi}{dr^2} - \frac{\sin(2\psi)}{4} \left(\frac{d\psi}{dr} \right)^2 + \frac{\cos^2 \psi}{r} \frac{d\psi}{dr} - \frac{\sin(2\psi)}{2r^2} \\ - \frac{\delta p r}{2k \cos \psi} - \frac{\sin \psi}{2 \cos \psi} \left(\frac{\sin \psi}{r} - c_0 \right)^2 - \frac{\lambda \sin \psi}{k \cos \psi} = \frac{C}{r \cos \psi}, \end{aligned} \quad (5)$$

where C is a constant of integration. It is still a rather complicated equation and does not belong to any known type of well-studied differential equation in mathematics.

Under the conditions that both the surface tension λ and the osmotic pressure difference δp are zero, i.e.,

$$\lambda = \delta p = 0, \quad (6)$$

an analytic CBS solution for the Eq.(3) [8,11], or Eq. (5) with $C = 2c_0$, is

$$\sin \psi = r/R_0 + c_0 r \ln r, \quad \text{or equivalently,} \quad \sin \psi = c_0 r \ln(r/r_m), \quad (7)$$

where R_0 is an arbitrary constant and $r_m = \exp(-1/(c_0 R_0))$. When we first obtained this solution [8,11], we concentrated on the fact that it can be used to represent the CBS of usual red blood cells [11]. In fact, by adjusting parameter c_0 in the interval $(-\infty, \infty)$, the formula (7) can give a family of shapes, which is what we are going to analyze in detail. For sake of convenience, we mainly use the first form of the CBS solution (7) with $R_0 = 1$.

III. ALL POSSIBLE SHAPES IN THE CBS SOLUTION

Before presenting the shapes, we would like to make two comments on how to characterize the shapes. First, for each shape, we will give both the parameterization and the interval of $r \in [0, \infty)$ in which the shape appears. This is because that there may be different shapes represented by the same parameterization in distinct intervals of $r \in [0, \infty)$ as long as in the intervals $|\sin \psi(r)| \leq 1$ are satisfied. Second, even the scale invariance will be fully studied in section V, we will follow the usual usage [10] to give for each shape the scale invariant $c_0 r_s$, in which $r_s = \sqrt{A/4\pi}$ with A denoting the area of the surface of the shape. Unless specially mentioned and discussed, that the normals of the surface point outwards for closed shapes is always implied.

All possible types of shapes represented by Eq. (7) are listed in the following.

i) The flat plane (trivial case) with $c_0 r_s = 0$:

$$\sin \psi = 0, \quad r \in [0, \infty]. \quad (8)$$

ii) The sphere with $c_0 r_s = 0$:

$$\sin \psi = r/R_0, \quad r \in [0, R_0]. \quad (9)$$

iii) The prolate ellipsoid. A typical shape with $c_0 r_s = -0.72$ is shown in FIG.2(a) and one of its parameterization is

$$\sin \psi = r - 0.6r \ln r, \quad r \in [0, 1]. \quad (10)$$

Another parameterization representing the same shape is $\sin \psi = r - 1.85r \ln r$, $r \in [0, 0.324]$. The parameterization $\sin \psi = r + 4.063r \ln r$, $r \in [0, 0.148]$ represents the same shape but with inwards pointing normal.

iv) The capped cylinder. A typical shape with $c_0 r_s = -2.06$ is shown in FIG.2(b) and one of its parameterization is

$$\sin \psi = r - 0.99r \ln r, \quad r \in [0, 1]. \quad (11)$$

Another parameterization representing the same shape is $\sin \psi = r - 1.01r \ln r$, $r \in [0, 0.980]$. The parameterization $\sin \psi = r + 3.5913r \ln r$, $r \in [0, 0.275]$ represents the same shape but with inwards pointing normal.

v) The oblate ellipsoid. A typical shape with $c_0 r_s = 0.46$ is shown in FIG.2(c) and its parameterization is

$$\sin \psi = r + 0.5r \ln r, \quad r \in [0, 1]. \quad (12)$$

vi) The CBS. A typical shape with $c_0 r_s = 1.51$ is shown in FIG.2(d) and its parameterization is

$$\sin \psi = r + 1.8r \ln r, \quad r \in [0, 1]. \quad (13)$$

vii) The self-intersecting inverted CBS. A typical shape with $c_0 r_s = 2.72$ is shown in FIG.2(e) and its parameterization is

$$\sin \psi = r + 3.2r \ln r, \quad r \in [0, 1]. \quad (14)$$

To note that in this case, the outside of this shape can be defined but we can not let the normal always point outwards using a single parameterization (14). The normal of the parameterization (14) points outwards only at the surface of the torus part.

viii) The self-intersecting nodoidlike cylinder. This situation was discussed in previous paper [12]. We add a typical figure, FIG.2(f), in this paper for completeness. The cylinder is infinitely long with periodic packing, along the rotational axis, of a basic unit in which self-intersecting occurs once. We plot the basic unit only. We use the surface of the basic unit to calculate r_s and the shape has $c_0 r_s = 3.28$. Its parameterization is

$$\sin \psi = r + 3.60r \ln r, \quad r \in [0.301, 1]. \quad (15)$$

The normal of this parameterization points outwards only at the surface of the torus part also. To note that the same parameterization $\sin \psi = r + 3.60r \ln r$ in interval $r \in [0, 0.257]$ gives a capped cylinder but its normal points inwards.

These eight shapes consist of all possible types of shapes containing in the solution. From the parameterizations of the these shapes, one may have noticed two facts that the spontaneous curvatures of all shapes are within a very narrow domain instead of infinite domain of $c_0 \in (-\infty, \infty)$, and a single shape may have different parameterizations. Explanations of these facts will be given in next section by both qualitative and quantitative studies of the CBS solution.

IV. A QUANTITATIVE STUDY OF SHAPES IN THE CBS SOLUTION

All the closed shapes (ii)-(vii) presented in last section can be grouped into two branches: The prolate ellipsoid including (ii)-(iv) and oblate ellipsoid branch including (ii), (v)-(vii), and these two branches are bifurcated from a sphere (ii). It is easily understandable if looking into the CBS solution (7) $\sin \psi = r/R_0 + c_0 r \ln r$. When $R_0 > 0$ and $c_0 = 0$, this form gives nothing but sphere of radius R_0 . Then when c_0 is a small quantity, positive c_0 leads to oblate ellipsoid and negative c_0 leads to prolate ellipsoid respectively. What if c_0 is large is not so evident and needs some reasoning.

For analyzing how c_0 affects the shapes and the intervals of r such that $|\sin \psi(r)| \leq 1$, we use the parameterization $\sin \psi = r + c_0 r \ln r$, and sketch the relation of $\sin \psi$ with positive c_0 vs. r in FIG.3.

From this figure, we see that $\sin \psi = r + c_0 r \ln r$ is a single-valued and monotonous function of r ; and it reaches its extremum at point r_2 which satisfies

$$\frac{d \sin \psi}{dr} = 1 + c_0 + c_0 \ln r_2 = 0, \quad i.e., \quad r_2 = \exp\left(-\frac{1 + c_0}{c_0}\right). \quad (16)$$

The extremum value of $\sin \psi(r_2)$ is

$$\sin \psi(r_2) = -r_2 c_0 = -c_0 \exp\left(-\frac{1 + c_0}{c_0}\right), \quad (17)$$

which is negative for positive c_0 and vice verse. Taking the positive c_0 as an example in FIG. 3, corresponding to different c_0 , shapes can appear in different intervals of r . There are three different cases of $c_0 \in [0, \infty)$. i) When c_0 is critical such that $\sin \psi(r_2) = -1$, we have $c_0 = c_r \approx 3.59112$ from Eq.(17). The meridian principal curvature vanishes at point r_2 as $c_2 = d \sin \psi / dr = 0$: it is the unphysically infinitely long capped cylinder with radius $r_2 = 1/c_0 = 0.278$ from Eq. (17). ii) When $c_0 < c_r$, we have $\sin \psi(r_2) > -1$ and shapes appear in one interval $[0, r_4]$ in which r_4 are the equatorial radii of the shapes such that $\sin \psi(r_4) = 1$. Along the increase of r from 0 to r_4 , the tangent angle $\psi(r)$ decreases from zero and reaches its minimum at point r_2 , then increases monotonously and reaches its maximum value $\psi = \pi/2$ at point r_4 . These shapes certainly belong to the oblate ellipsoid branch, and their normals point outwards from Eq. (4). iii) When $c_0 > c_r$, we have $\sin \psi(r_2) < -1$, shapes can appear in two distinct intervals $[0, r_1]$, in which r_1 are the equatorial radii of the shapes such that $\sin \psi(r_1) = -1$, and $[r_3, r_4]$, because in both intervals $|\sin \psi(r)| \leq 1$ is satisfied. In interval $[0, r_1]$, the tangent angle $\psi(r)$ decreases from zero and terminates at $\psi(r_1) = -\pi/2$. These shapes certainly belong to the prolate ellipsoid branch, but the normals point inwards since $-1 \leq \sin \psi(r) \leq 0$ holds for whole interval $r \in [0, r_1]$. In distinct interval $[r_3, r_4]$, numerical studies show that only the self-intersection nodoidlike cylinder appears.

In fact, using the parameterization $\sin \psi = r/R_0 + c_0 r \ln r$, each shape with a c_0 outside the domain $(-1, c_r)$ can be found an identical shape with a value of c_0 within the domain $(-1, c_r)$. For demonstrating this fact, we resort to the second form of the CBS solution $\sin \psi = c_0 r \ln(r/r_m)$ in Eq. (7). Two parameterizations $c_0 r \ln(r/r_m)$ and $-c_0 r \ln(r/r_m)$ represent the same shape, but one's normal is opposite to another's from Eq.(4). If requiring that the

normal points outwards, one of these two parameterizations must be eliminated. Furthermore we have a simplified form

$$\begin{aligned}\sin \psi &= c_0 r \ln(r/r_m) \\ &= (c_0 r_m)(r/r_m) \ln(r/r_m) \\ &= c'_0 x \ln x,\end{aligned}\tag{18}$$

where $x = r/r_m$ is the dimensionless length, and $c'_0 = c_0 r_m = c_0 \exp(-1/(c_0 R_0))$ is a dimensionless spontaneous curvature. One can find that the c'_0 in two separate domains $c'_0 \in (-\infty, -e)$ and $c'_0 \in [0, e)$, in which e is the base of the natural logarithm, suffice to give all possible shapes with normals pointing outwards in the CBS solution. When $c'_0 = \pm e$, the shapes are unphysically infinitely long capped cylinders. From the relation $c'_0 = c_0 \exp(-1/(c_0 R_0))$ and letting $R_0 = 1$, all shapes can be mapped into a single domain $c_0 \in (-1, c_r)$ in parameterization $\sin \psi = r/R_0 + c_0 r \ln r$. This is why there are only a few of spontaneous curvature c_0 within a narrow domain in the last section are sufficient to give all possible types of shapes in the CBS solution, i.e., why each shape with a c_0 outside the domain $(-1, c_r)$ can be found an identical shape with a value of c_0 within the domain $(-1, c_r)$.

In addition to the above qualitative analyses, numerical method will be used to characterize quantitatively the shapes in whole domain $c_0 \in (-\infty, \infty)$. We introduce two ratios, semi-axis ratio $z(r_0)/r_0$ and reduced radius ratio r_v/r_s . The so-called semi-axis $z(r_0)$ is defined by the half of the distance of two poles of a vesicle in the symmetrical axis z , which is

$$z(r_0) - z(0) = - \int_0^{r_0} \tan \psi(r) dr,\tag{19}$$

where r_0 is the equatorial radius of the vesicle satisfying $\sin \psi(r_0) = \pm 1$. The ratios $z(r_0)/r_0$ are plotted by dashed lines in FIG. 4. From FIG. 4(b), the c_0 approaches -1 and c_r , the ratio $z(r_0)/r_0$ approaches infinity: the shapes are infinitely long capped cylinders with radii 1 and 0.278 respectively. When c_0 increases from -1 to c_r , the ratio decreases monotonously. We have in sequence the capped cylinder, the prolate ellipsoid and the sphere of unit radius at $c_0 = 0$, the oblate ellipsoid with a small positive c_0 , the CBS and the center of the CBS touches at $c_0 = 2.4288$, then self-intersecting inverted CBS. From FIG. 4(a) and FIG. 4(c), we clearly see that when $c_0 < -1$ or $c_0 > c_r$, the ratios $z(r_0)/r_0$ are greater than 1. We have in sequence the capped cylinder, the prolate ellipsoid and the quasi-sphere with increasing $|c_0|$. When $|c_0|$ approaches infinity, the constraint $|\sin \psi(r)| \leq 1$ means that r_1 , cf. FIG. 3, must be very small. Thus we have approximately $\sin \psi(r) \simeq \mp c_0 r$ for positive and negative c_0 respectively using L' Hospital method. It implies that we will have sphere again. All these shapes are closed and appear in intervals of r including the point $r = 0$, which are physically interesting and are plotted in the FIG. 4. When $c_0 < -1$ or $c_0 > c_r$, in intervals $[r_3 > 0, r_4]$ (cf. FIG. 3), we have the self-intersecting nodoidlike cylinders, which are less physically interesting and have not been plotted in the FIG. 4. As pointed out in [12], along with the increasing $|c_0|$, the number of self-intersections in unit length increases and it approaches a quasi-torus as $|c_0|$ approaches ∞ . In fact, when $-1 < c_0 \leq 0$, the self-intersecting nodoidlike also appear in the intervals $[r_3 > 0, r_4]$, but along with the decreasing $|c_0|$, the number of self-intersections in unit length increases.

The second ratio is r_v/r_s , in which r_v is defined by the radius of the sphere having the same volume V of a vesicle and r_s the radius of the sphere having the same area A of the vesicle. The volume V and area A are

$$V = 4\pi \int_0^{r_0} \frac{r(z(r) - z(0))}{\cos \psi} dr,\tag{20}$$

$$A = 4\pi \int_0^{r_0} \frac{r}{\cos \psi} dr.\tag{21}$$

Undoubtedly, we have $r_v/r_s \leq 1$ and the equality holds for sphere only. The ratio is plotted by dot-dashed lines in FIG. 4.

The scale invariant $c_0 r_s$ is plotted by thin solid lines in FIG. 4. In FIG. 4(c), we plot both $c_0 r_s$ (above the c_0 axis) and $-c_0 r_s$ (below the c_0 axis) by the same thin solid lines, in order to see the fact that each shape with a $c_0 \in (-\infty, -1)$ is identical to a shape with a $c_0 \in (c_r, \infty)$ and vice versa. But the normals of shapes parameterized by $\sin \psi = r + c_0 r \ln r$ with $c_0 \in (c_r, \infty)$ point inwards.

From both the qualitative and quantitative studies in this section, we can draw a conclusion that all possible closed shapes in the CBS solution (8) are, along with c_0 increasing from -1 to c_r , the capped cylinder, the prolate ellipsoid, the sphere, the oblate ellipsoid, the CBS, and the self-intersecting inverted CBS.

V. THE SCALE INVARIANCE OF THE ENERGY AND THE SHAPE WITH MINIMUM ENERGY

An important property of the local curvature energy is its scale invariance. This energy does not depend on the size of the vesicle but only on its shape [10]. If \mathbf{R} is a solution with a local curvature energy, the rescaled shape $\mathbf{R} \rightarrow \mathbf{R}/k$ with $k > 0$, and consequently $(c_1, c_2, c_0, dA) \rightarrow (kc_1, kc_2, kc_0, dA/k^2)$, is also a solution with the same local curvature energy. Two parameterizations of the CBS solution (8) having manifest scale invariance are

$$\sin \psi(r) = r/R_0 + c_0 r \ln(r/r_0), \quad \text{and} \quad \sin \psi(r) = c_0 r \ln(r/r_0), \quad (22)$$

in which r_0 is a constant with length unit as r or R_0 . It is evident that the two products $c_0 r_s$ and $c_0 r_v$ are two scale invariants independent of a particularly chosen parameterization. We used two particular parameterizations, $\sin \psi(r) = r/R_0 + c_0 r \ln r$ and $\sin \psi(r) = c_0 r \ln r$, to search for the minimum energy shape. Both gives the same result $c_0 r_s = 1.04$ and $c_0 r_v = 1.00$. The minimum energy is 0.480; hereafter we take the energy of sphere $8\pi k$ as the energy unit. Surprisingly, the CBS with touching center at $c_0 = 2.4288$ has energy 1.00. In FIG. 4 (b), the thick solid line shows that there is a energy minimum shape with $c_0 = 1.200$: it is a CBS. In general, the oblate ellipsoids including the CBS have lower energy than other shapes including the sphere, prolate ellipsoid and the self-intersecting inverted CBS have.

VI. A COMPARISON OF OUR RESULTS WITH THE PREVIOUS EXPERIMENTAL AND THEORETICAL RESULTS

Even all the previous numerical studies concentrated on the solution of equation when $C = 0$ of Eq. (5), the obtained shapes [10,16] included all the eight shapes above. And also, all these eight shapes except the self-intersecting cases have been observed in laboratory [16–18].

Since our solution belongs to the situation $C \neq 0$ of Eq.(5), our results coincide with the known theoretical results in one respect but differ from in the other. First, our approach supports the conclusion that the prolate ellipsoids may have higher energy than the oblate ones have [4]. However, the standard instability analysis of a sphere starts from a slightly deformed sphere of parameterized form $r = R_0 + \sum a_{lm} Y_{lm}(\theta, \phi)$ where a_{lm} is a set of small parameters corresponding to spherical harmonics $Y_{lm}(\theta, \phi)$. For small a_{lm} , for example the only nonvanishing $a_{2,0}$ satisfying $|a_{2,0}| \ll R_0/2$, the ellipsoids have C^∞ contour curves. But our ellipsoids have only C^1 contour curves. We must stress that the C^1 continuity suffices to ensure that the membranes are free from any force acting on the any point, otherwise the contour curve may be C^0 . The second derivative of $z(r)$ with respect to r is singular at point $r = 0$. One may feel uneasy of this singularity. In fact, it relates to energy density only, and the total energies $(1/2)k \int (c_1 + c_2 - c_0)^2 dA$ are limited as shown in FIG.4. Second, the infinitely long capped cylinders appear when $c_0 = -1$ and $c_0 = c_r$, and they correspond the infinite energy states, as shown by thick solid lines in FIG.4 (a)-(c). From our results, the phases between the two sides of $c_0 = -1$ and $c_0 = c_r$ are separate. The latter c_r distinguishes a oblate ellipsoid and a prolate ellipsoid phase; it is the same situation in the known phase diagram [10]. However when c_0 changes from $c_0 < c_r$ to $c_0 > c_r$, the normal changes its direction from pointing outwards to pointing inwards. It seems that the membrane takes a global flip-flop procedure. But no such procedure takes place when c_0 changes from $c_0 < -1$ to $c_0 > -1$ even the transitions are also discontinuous. Third, there is an interesting number appeared both in our results and the previous ones, $c_0 R_0 = 1.200$. We see that from the FIG. 4(b) when $c_0 R_0 = 1.200$ where $R_0 = 1$ in our parameterization, the CBS has the minimum energy. In the usual instability analysis of a sphere via infinitesimal deformation, the infinitesimally deformed oblate shape has the lower energy and more stable than the infinitesimally deformed prolate one whenever $c_0 R_0 < -1.2$ [4].

VII. CONCLUSION

An analytic solution for Helfrich spontaneous curvature membrane model [8,11], which has a conspicuous feature of representing the circular biconcave shape, is systematically studied in this paper. Results show that the solution in fact describes a family of shapes, which can be classified as: i) the flat plane (trivial case), ii) the sphere, iii) the prolate ellipsoid (FIG.2(a)), iv) the capped cylinder (FIG.2(b)), v) the oblate ellipsoid (FIG.2(c)), vi) the CBS (FIG.2(d)), vii) the self-intersecting inverted CBS (FIG.2(e)) and viii) the self-intersecting nodoidlike cylinder (FIG.2(f)). All these shapes have been found in numerical solutions of Eq. (5) with $C = 0$ [9]. Except the self-intersecting cases, they all have real correspondence in vitro and in vivo on vesicle shapes [16–18]. The closed shapes ii)-vii) form two

separate prolate and oblate ellipsoid branches which are bifurcated from a sphere. The oblate ellipsoids including CBS have lower energy than the prolate ellipsoids including sphere, and a CBS with $c_0 r_v = 1.00$ has the lowest energy. The usual instability analysis of sphere leads to that the least stable shapes are prolate and oblate ellipsoid branches [4,19], but it is the first time to give an explicit parameterization to show how these two branches come out gradually and analytically.

We are indebted to Professors. Peng Huan-Wu and Zheng Wei-Mou for enlightening discussions. This subject is supported by National Natural Science Foundation of China.

** e-mail address: liuqh@itp.ac.cn

- [1] P.B.Canham, J. Theor. Biol. **26**, 61(1970)
- [2] W. Helfrich, Z.Naturforsch **28c**, 693 (1973).
- [3] H. J. Deuling and W. Helfrich, Biophys. J. **16**, 861 (1976); J. Phys. France **37**, 1335 (1976)
- [4] Ou-Yang Zhong-Can and W. Helfrich, Phys. Rev. Lett. E **59**, 2486 (1987); Phys. Rev. A, **39**, 5280 (1989)
- [5] Ou-Yang Zhong-Can, Phys. Rev. A **41**, 4517 (1990);
- [6] M. Mutz and D. Bensimon, Phys. Rev. A **43**, 4525 (1991);
- [7] Hu Jian-Guo and Ou-Yang Zhong-Can, Phys. Rev. E **47**, 461 (1993).
- [8] H. Naito, M.Okuda and Ou-Yang Zhong-Can, Phys. Rev. E **48**, 2304 (1993).
- [9] W. M. Zheng and J. X. Liu, Phys. Rev. E **48**, 2856 (1993).
- [10] U. Seifert, Phys. Rev. **44**, 1182(1991), Adv. Phys. **46**, 13(1997), and U. Seifert and R. Lipowsky, in Handbook of Biological Physics (Vol. I) edited by R. Lipowsky and E. Sackman (Elsevier Science, Amsterdam, 1995)
- [11] H. Naito, M.Okuda and Ou-Yang Zhong-Can, Phys. Rev. E **54**, 2816 (1996).
- [12] H. Naito, M. Okuda and Ou-Yang Zhong-Can, Phys. Rev. Lett. **74** 4345 (1995)
- [13] J. C. Nitsche, Lectures on Minimal Surfaces (Vol. 1), (Cambridge University Press, Cambridge, 1989).
- [14] A. I. Bobenko, Math. Ann. **290**, 209 (1991); U. Pinkall and I. Sterling, Math. Intell. **9**, 38 (1987)
- [15] E. T. Whittaker and G. N. Watson, A Course of Modern Analysis (4th. ed), (Cambridge University Press, Cambridge, 1940);
- [16] H.-H. Dobreiner, E. Evans, M. Krauss, U. Seifert, and M. Wortis, Phys. Rev. E **55**, 4458(1997),
- [17] T. Umeda, H. Nakajima, and H. Hotani, J. Phys. Soc. Japan **67**, 682(1998)
- [18] M. Bessis, Living Blood Cells and their Ultrastructure (Tran. by R. I. Weed) (Spring-Verlag, Berlin, 1973), Red Cell Shape (Physiology· Pathology· Ultrastructure) (Spring-Verlag, Berlin, 1973)
- [19] M. A. Peterson, Phys. Rev. A **39**, 2643(1989)

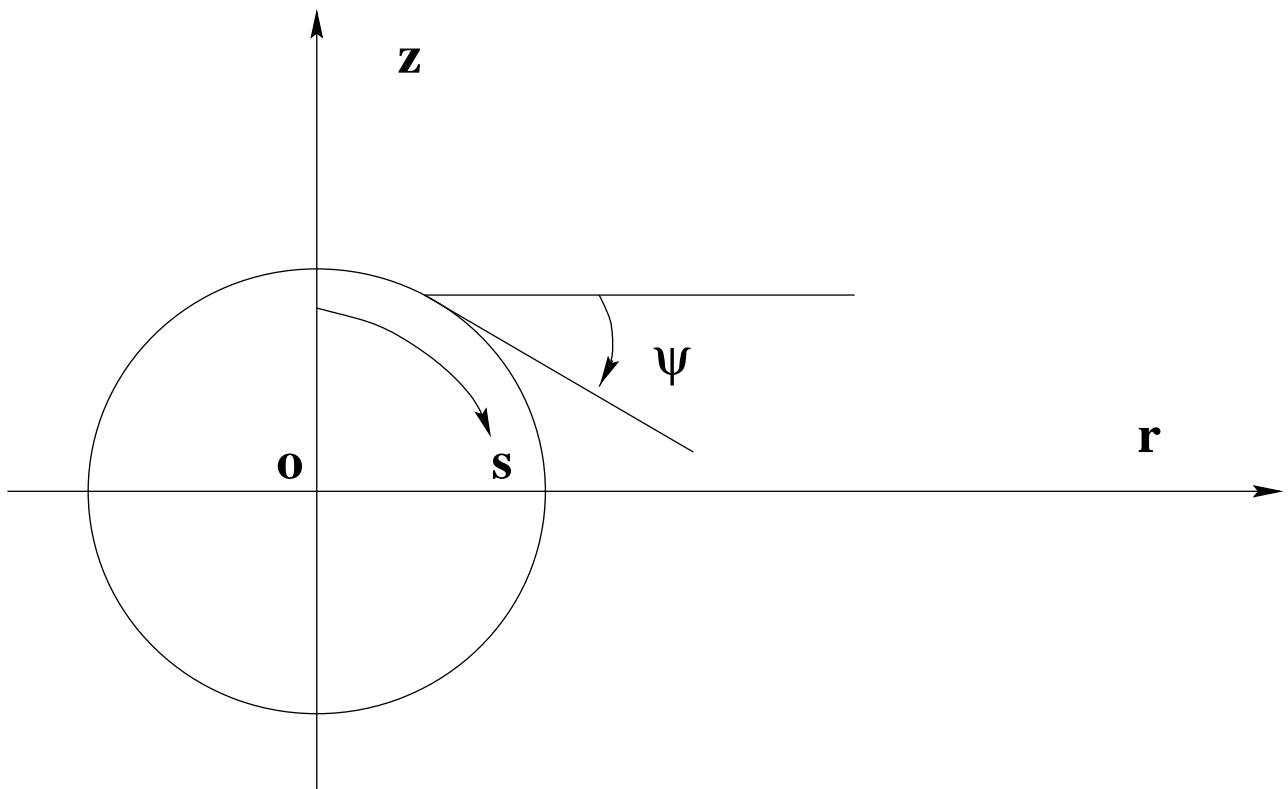


FIG. 1. Sign convention. Four arrows mean positive directions for rotational axis z and radial axis r , tangent angle ψ and arclength s , respectively. At the north pole both the arclength s and the tangent angle ψ take zero values.

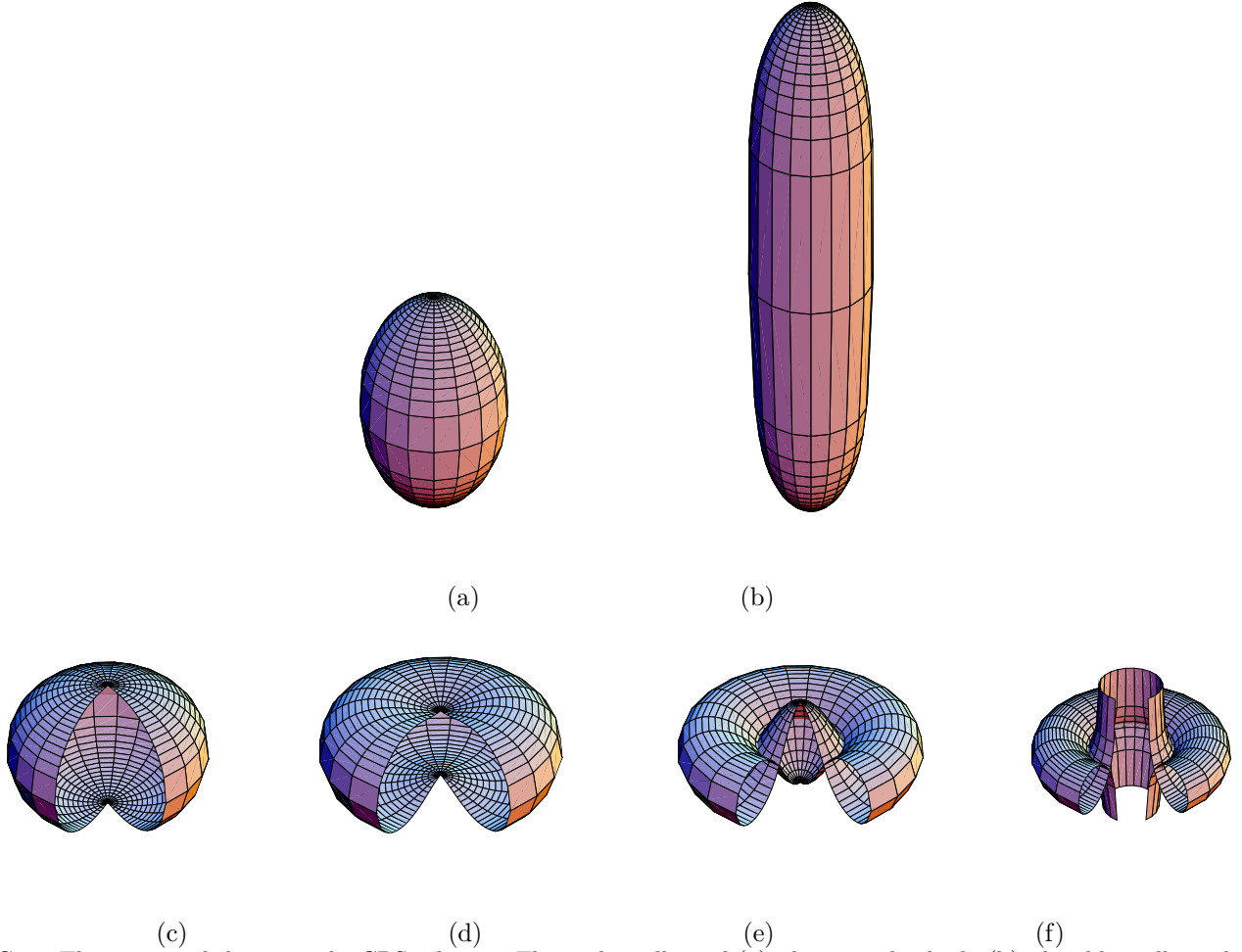


FIG. 2. The nontrivial shapes in the CBS solution. The prolate ellipsoid (a), the capped cylinder (b), the oblate ellipsoid (c), the CBS (d), the self-intersecting inverted CBS (e) and the self-intersecting nodoidlike cylinder (f).

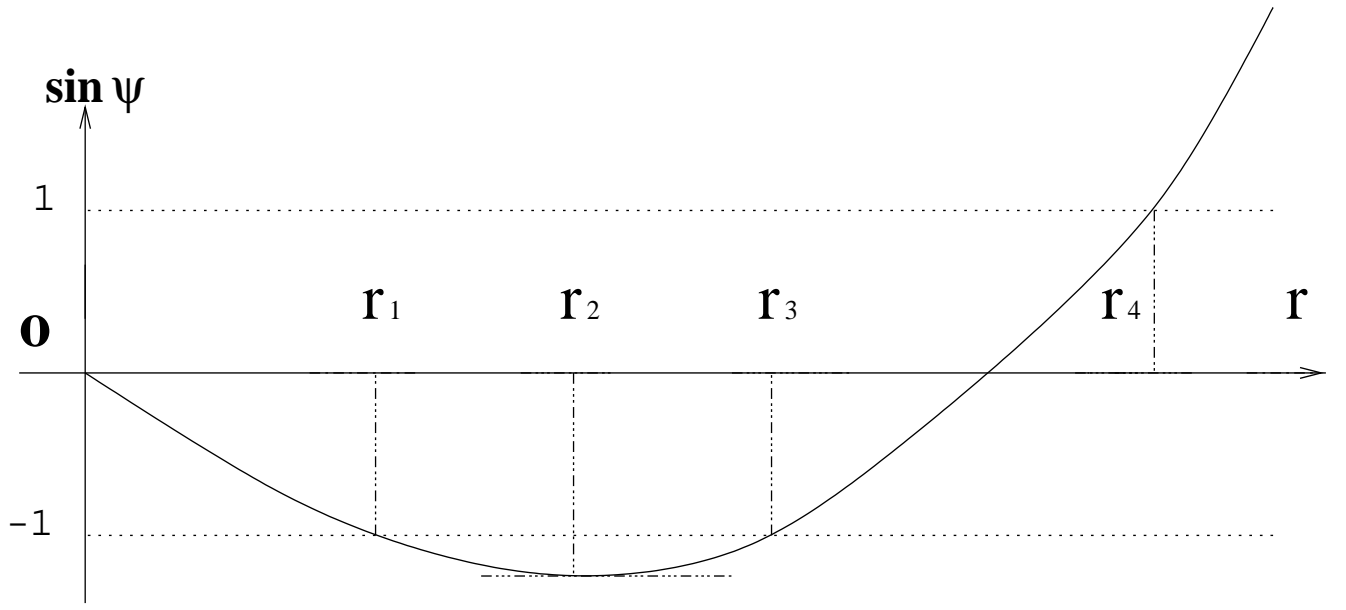


FIG. 3. The relation of $\sin \psi(r)$ vs. r and the intervals where the shapes appear. When $0 < c_0 < c_r$, $-1 < \sin \psi(r_2) < 0$, shapes appear in $[0, r_4]$. When $c_0 \geq c_r$, $\sin \psi(r_2) \leq -1$, shapes appear in two distinct intervals $[0, r_1]$ and $[r_3, r_4]$.

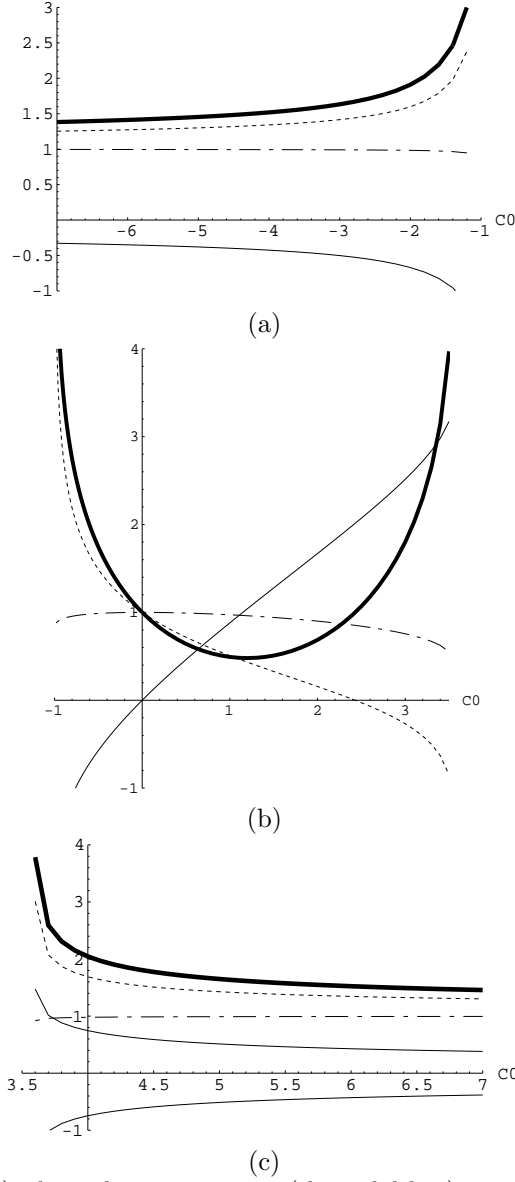


FIG. 4. The energy (thick solid line), the scale invariant $c_0 r_s$ (thin solid line), two ratios $z(r_0)/r_0$ (dashed line) and r_v/r_s (dot-dashed line), in three domains $-7 \leq c_0 \leq -1.2$ (a), $-0.98 \leq c_0 \leq 3.5$ (b), and $3.6 \leq c_0 \leq 7$ (c), for closed shapes. The bending elastic modulus k used to scale the energy of a sphere to unit. All quantities in four curves are dimensionless. In order to see clearly that fact that a shape with an exclusive value of $c_0 \in (-\infty, -1)$ and a shape with an exclusive value of $c_0 \in (c_r, \infty)$ are identical except that the normals point inwards and outwards respectively, in last figure (c), we plot both $c_0 r_s$ (above the c_0 axis) and $-c_0 r_s$ (below the c_0 axis) by the same thin solid lines. We can also see that all shapes with $c_0 \in (-\infty, -1)$ and $c_0 \in (c_r, \infty)$ have their corresponding identical shapes with $c_0 \in (-1, 0)$. A single domain $c_0 \in (-1, c_r)$ thus suffices to give all shapes.